

# Long-Range Interaction Between Adatoms in Graphene

Andrei V. Shytov,<sup>1</sup> Dmitry A. Abanin,<sup>2</sup> and Leonid S. Levitov<sup>3</sup>

<sup>1</sup>*Department of Physics, University of Utah, Salt Lake City, UT 84112*

<sup>2</sup>*Department of Physics, Jadwin Hall, Princeton University, Princeton, NJ 08544*

<sup>3</sup>*Department of Physics, Massachusetts Institute of Technology, Cambridge MA 02139*

We present a theory of electron-mediated Casimir-like interaction between adatoms in graphene, in which massless fermions play the role of photons. In the case of resonant scattering, relevant for hydrogenated graphene, a long-range  $1/r$  interaction is found. The interaction is an attraction or a repulsion depending on whether the adatoms reside on the same sublattice or on different sublattices, with attraction dominating for adatoms randomly distributed over both sublattices. The attractive nature of these forces creates an instability under which adatoms tend to aggregate. This behavior is crucial for understanding macroscopic properties of hydrogenated graphene.

PACS numbers:

High electron mobility and other attractive characteristics make graphene a strong candidate for replacing silicon in future electronic devices [1]. Functionalizing graphene by controllable oxidation [2, 3] or hydrogenation [4, 5] can change its properties in new, unexpected ways. In particular, hydrogenated graphene behaves as a semiconductor [5], with metallic properties fully recovered after annealing. When hydrogen adatoms bind to graphene, the orbital state of each functionalized carbon atom changes from  $sp^2$  to  $sp^3$  configuration [6]. The resulting hydrocarbon compound, graphane, is predicted to be a semiconductor with a few eV energy gap at a full hydrogen coverage [7, 8].

This provides a unique tool for controlling electronic properties of this material, and also poses fundamental questions in basic science of nano-carbon. In order to describe hydrogen adatoms at a finite concentration, and to understand their physical state and properties, it is important to analyze the interaction between the adatoms. Here we focus on the interaction mediated by the massless Dirac electrons scattering on the adatoms. Resonant scattering on the midgap states, or zero-modes, localized on adatoms [9, 10, 11], leads to dramatic enhancement of interaction. We find that the interaction energy falls off very slowly, approximately as inverse distance between the adatoms,  $U(r) \sim r^{-1}$ . The sign of interaction depends on the sublattice type: two atoms residing on different sublattices (*A* and *B*) attract, whereas atoms on the same sublattice repel [see Eqs.(11),(13)].

The  $r^{-1}$  interaction is stronger than the long-range interaction between adatoms on surfaces of metals [12, 13, 14], which is of a Friedel-oscillation (FO) character. The FO interaction falls off as  $r^{-2}$  when it is mediated by electronic states on the surface, and as  $r^{-3}$ , when mediated by the states in the bulk [15, 16]. The FO interaction can occur in graphene [17]. Long-range interaction can lead to fascinating collective behavior of adatoms, such as self-organization into chains [14] and superlattices [18].

The interaction analyzed in this work can be interpreted as a fermionic Casimir effect. One way to under-

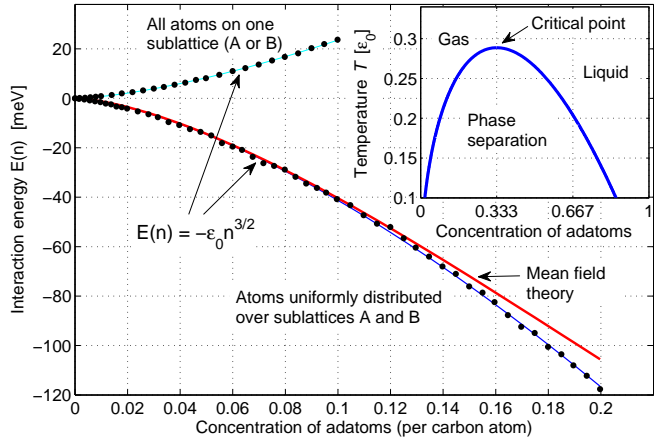


FIG. 1: Electron-mediated interaction between adatoms in graphene (numerical results and mean field theory). The interaction is positive when adatoms are randomly placed on one of the sublattices (repulsion), and is negative when they are equally distributed among both sublattices (attraction). Energy density per carbon atom *v*s. the fraction of hydrogenated atoms *n* follows the relation (1) with the best fit values  $\epsilon_0 = -0.75$  eV (top curve) and  $\epsilon_0 = 1.3$  eV (bottom curve). Analytic result derived from a mean field theory, Eq.(18), is shown by red line. Inset: Attracting adatoms tend to aggregate. Phase diagram obtained from the free energy (19) is shown.

stand the origin of the Casimir interaction between two bodies, e.g. atoms, is in terms of scattering of photon zero-point fluctuations (or, virtual photons). For each of the bodies, in the presence of the second body, angular distribution of the flux of incident virtual photons is somewhat anisotropic, giving rise to a net attraction force. This interpretation of the Casimir effect highlights its generic character (fermionic Casimir effect was recently analyzed in one-dimensional systems [19]).

We find that attraction between atoms on different sublattices is stronger by a logarithmic factor than repulsion within the same sublattice. The net interaction of atoms equally distributed among the two sublattices

is thus an attraction, characterized by the energy density

$$E(n) = -\varepsilon_0 n^{3/2}, \quad \varepsilon_0 \approx 1.3 \text{ eV}, \quad (1)$$

per carbon atom (see Fig.1), where  $n$  is the fraction of hydrogenated carbon atoms. The prefactor in (1) may have a weak logarithmic dependence on  $n$ .

We emphasize that the interaction energy in this case cannot be treated as a sum of pairwise two-particle interactions (indeed, summing  $1/r$  interactions over the entire space would give a divergence). The situation resembles that of Casimir forces, which are of an essentially non-pairwise nature. To treat the interaction mediated by electrons one must account for the change in electronic states at the energies  $\varepsilon \lesssim \hbar v_0 n^{1/2}$ , resulting from electron scattering on the adatoms ( $v_0$  is the electron Fermi velocity). This leads to interaction energy per adatom of order  $\hbar v_0 / r$ , with  $r = n^{-1/2}$  the typical distance between adatoms, in agreement with  $n^{3/2}$  scaling, Eq.(1).

Attraction can lead to instability of a homogeneous phase and adatom aggregation, which we analyze below. Characteristic time scales for such processes should depend on the rates of adsorption and desorption rather than diffusion. While diffusion of physisorbed hydrogen on graphite persists down to  $T = 0$  [20], a recent transmission electron microscopy (TEM) study of graphene reports stable and well-localized hydrogen adatoms [21]. This is in agreement with the picture of chemisorbed adatoms strongly bound to the surface. Compression of the graphene lattice, resulting from attraction between such adatoms, may explain the unexpected reduction of the lattice constant, measured by TEM diffraction [5], which is at odds with first-principles calculations [8].

Interaction between hydrogen adatoms could also result from corrugation of the graphene sheet caused by the stress around tetrahedral  $sp^3$  bonds. Numerical evidence suggests, however, that such corrugation is limited to the range of at most a few lattice constants[8], rendering this type of interaction effectively short-ranged.

The Hamiltonian of electrons scattering on impurity potential is a sum of the kinetic and potential energies, in the tight-binding approximation given by

$$H = \sum_{\mathbf{k}} (t_{\mathbf{k}} \psi_{\mathbf{k},A}^\dagger \psi_{\mathbf{k},B} + \text{h.c.}) + \sum_{\mathbf{x}, \alpha=A,B} u_\alpha(\mathbf{x}) \psi_{\mathbf{x},\alpha}^\dagger \psi_{\mathbf{x},\alpha}. \quad (2)$$

Here  $u_{A(B)}(\mathbf{x})$  is adatoms' potential on sublattices  $A(B)$ , and  $t_{\mathbf{k}} = t_0(1 + e^{-i\mathbf{k}\mathbf{e}_1} + e^{-i\mathbf{k}\mathbf{e}_2})$ , with  $t_0 \approx 3.1 \text{ eV}$  the hopping amplitude and  $\mathbf{e}_{1(2)}$  the basis vectors (see Fig.2b).

The interaction between adatoms can be analyzed using thermodynamical potential, written in terms of the electron Matsubara Greens function,  $\Omega = T \sum_{\varepsilon_n} \text{Tr} \ln G$  [22]. For two adatoms, we write  $G^{-1} = G_0^{-1} - V_1(\mathbf{x} - \mathbf{x}_1) - V_2(\mathbf{x} - \mathbf{x}_2)$  and resum perturbation series in terms of the T-matrices, which describe scattering on each adatom,

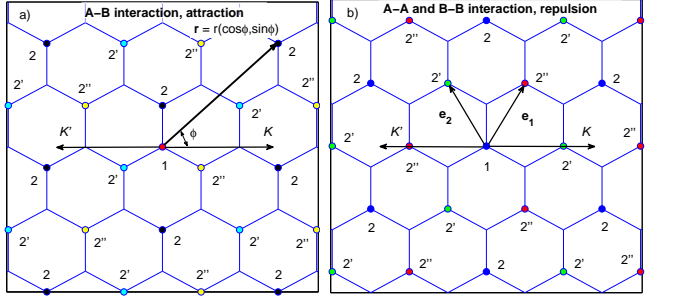


FIG. 2: Electron-mediated interaction between adatoms depends on the type of sublattice: atoms on different sublattices,  $A$  and  $B$ , attract (a), whereas atoms on the same sublattice repel (b) [see Eq.(11) and Eq.(13)]. The interaction is modulated by a prefactor which takes different values on the three sub-sublattices marked by  $2$ ,  $2'$  and  $2''$ : (a)  $|\sin(\mathbf{K}\mathbf{r} + \phi)| = |\sin \phi|, |\sin(\phi + \frac{2\pi}{3})|, |\sin(\phi - \frac{2\pi}{3})|$ ; (b)  $\cos^2(\mathbf{K}\mathbf{r}) = 1, \frac{1}{4}, \frac{1}{4}$ . The modulation results from interference between electronic states in valleys  $K$  and  $K'$ .

to obtain the interaction energy

$$\Omega = -T \sum_{\varepsilon_n} \text{Tr} \ln (1 - T_1 G_{12} T_2 G_{21}). \quad (3)$$

Here  $G_{12}$  is the free-particle Greens function in position representation, evaluated between the points  $\mathbf{x}_1$  and  $\mathbf{x}_2$  (similar representation was used recently in a study of Casimir forces [23, 24]).

In this paper we shall use the s-wave resonant scattering approximation,

$$T_0(i\varepsilon) = \frac{\pi v_0^2}{i\varepsilon \ln(W/|\varepsilon|) + \delta}, \quad |\delta| \ll W \approx 3t_0, \quad (4)$$

as appropriate for short-range scatterers at low energies. Here  $W$  is the electron half-bandwidth, and the parameter  $\delta$  describes detuning of resonance from the Dirac point. An expression of this form can be obtained for a delta-function potential,  $u(\mathbf{x}) = V \delta(\mathbf{x} - \mathbf{x}_1)$ , in which case the T-matrix is given by  $T(\varepsilon) = V / \left(1 + \frac{V}{\pi v_0^2} i\varepsilon \ln \frac{W}{|\varepsilon|}\right)$  [9, 10, 11]. For hydrogen adsorbed on graphene, the presence of a resonance peak close to the Dirac point, Eq.(4), was confirmed by first-principles calculations [6].

The real-space Greens function can be written as

$$G(i\varepsilon, \mathbf{r}) = - \int \frac{d^2 k}{(2\pi)^2} \frac{e^{i\mathbf{k}\mathbf{r}}}{\varepsilon^2 + |\mathbf{k}|^2} \begin{bmatrix} i\varepsilon & t_{\mathbf{k}} \\ t_{\mathbf{k}}^* & i\varepsilon \end{bmatrix}, \quad (5)$$

where the matrix accounts for the  $A$  and  $B$  sublattices. The Greens function takes on different form for the end points on different sublattices:

$$G(i\varepsilon, \mathbf{r}) = \begin{bmatrix} G_{AA} & G_{AB} \\ G_{BA} & G_{BB} \end{bmatrix}, \quad (6)$$

In the low-energy approximation we expand  $t_{\mathbf{k}}$  in the vicinity of points  $\mathbf{K}, \mathbf{K}' = -\mathbf{K}$  to obtain  $t_{\mathbf{k}} \approx v_0(\mp p_x -$

$ip_y$ ), where  $\mathbf{p} = \mathbf{k} \mp \mathbf{K}$  is the momentum relative to the  $\mathbf{K}$  ( $\mathbf{K}'$ ) point, and  $v_0 = \frac{3}{2}t_0$  is the Fermi velocity. Adding contributions of the states near  $\mathbf{K}$  and  $\mathbf{K}'$ , we obtain

$$G_{AA} = G_{BB} = -\frac{i\varepsilon \cos(\mathbf{Kr})}{\pi v_0^2} K_0(\varepsilon \tilde{r}), \quad \tilde{r} = \frac{r}{v_0}, \quad (7)$$

$$G_{AB} = -\frac{\varepsilon \sin(\mathbf{Kr} + \phi)}{\pi v_0^2} K_1(\varepsilon \tilde{r}), \quad (8)$$

where  $\phi$  is the angle between  $\mathbf{r}$  and  $\mathbf{K}$  (see Fig.2a), and  $K_{0,1}$  denote modified Bessel functions of the second kind,  $K_\nu(z) = \frac{\Gamma(\nu + \frac{1}{2}) 2^\nu}{\sqrt{\pi} z^\nu} \int_0^\infty \frac{\cos zt dt}{(1+t^2)^{\nu+1/2}}$ . The function  $G_{BA}$ , obtained in a similar manner, is

$$G_{BA} = -\frac{\varepsilon \sin(\mathbf{Kr} - \phi)}{\pi v_0^2} K_1(\varepsilon \tilde{r}). \quad (9)$$

Alternatively, this result for  $G_{BA}$  can be obtained using the relation  $G_{BA}(\mathbf{r}) = G_{AB}^*(-\mathbf{r})$ .

We first consider a pair of adatoms on different sublattices, one on  $A$  and one on  $B$  (see Fig.2a). In this case, the interaction energy is  $\Omega_{12} = -T \sum_{\varepsilon_n} \ln(1 - T_0^2(i\varepsilon) G_{AB}^2(i\varepsilon_n, \mathbf{r}))$ . In the limit of small temperature  $T \ll \hbar v_0/r$ , where  $r$  is the separation of adatoms, we can replace the sum  $T \sum_{\varepsilon_n}$  by an integral  $\int \frac{d\varepsilon}{2\pi}$ . Using Eq.(8), we find

$$\Omega_{12} = -\int \frac{d\varepsilon}{2\pi} \log \left( 1 + \frac{\sin^2(\mathbf{Kr} + \phi) K_1^2(\varepsilon \tilde{r})}{\log^2(W/\varepsilon)} \right). \quad (10)$$

The integral can be evaluated using the asymptotic formula  $K_1(x \ll 1) \approx 1/x$ . We replace  $\varepsilon$  in  $\ln(W/\varepsilon)$  by  $\varepsilon \approx v_0/r$  with logarithmic accuracy, and integrate over  $\varepsilon$  using the identity  $\int_0^\infty dx \ln(1 + u/x^2) = \pi\sqrt{u}$  to obtain

$$U_{AB}(r) = \Omega_{12} \approx -\frac{v_0 |\sin(\mathbf{Kr} + \phi)|}{r \log(r/\tilde{a})}, \quad \tilde{a} = v_0/W. \quad (11)$$

The interaction has negative sign, corresponding to *attraction* of adatoms.

Interestingly, due to the factor  $|\sin(\mathbf{Kr} + \phi)|$  in the above expression, the interaction *oscillates on the lattice scale*. This oscillation results from interference of the contributions due to fermions from  $K$  and  $K'$  valleys.

The meaning of the factor  $|\sin(\mathbf{Kr} + \phi)|$  can be seen more clearly by considering it separately on each of the three sub-sublattices, which have period  $\sqrt{3}$  times the period of the  $A$  or  $B$  sublattice (see Fig.2a). Since  $e^{i\mathbf{Kr}}$  takes values  $1, e^{2\pi i/3}$ , and  $e^{4\pi i/3}$ , the same on each of the three sub-sublattices, the angular dependence in Eq.(11) is given by  $|\sin(\phi)|$ ,  $|\sin(\phi + 2\pi/3)|$ , or  $|\sin(\phi + 4\pi/3)|$  in each of the three cases.

For a pair of adatoms residing on the same sublattice ( $A$  or  $B$ ), the interaction energy is  $\Omega_{12} = -T \sum_{\varepsilon_n} \ln(1 - (T_0(i\varepsilon_n) G_{AA}(i\varepsilon_n, \mathbf{r}))^2)$ , giving

$$\Omega_{12} = -\int \frac{d\varepsilon}{2\pi} \ln \left( 1 - \frac{\cos^2(\mathbf{Kr}) K_0^2(\varepsilon \tilde{r})}{\ln^2(W/\varepsilon)} \right). \quad (12)$$

We note a different sign under the log in this expression as compared to Eq.(10), which arises because  $G_{AA}$  is imaginary-valued, whereas  $G_{AB}$  is real-valued. The integral over  $\varepsilon$  is dominated by the region  $|\varepsilon| \lesssim v_0/r$ , since  $K_0(x)$  decreases exponentially at  $x \gtrsim 1$  [ $K_0(x \gg 1) \approx \sqrt{\frac{\pi}{2x}} e^{-x}$ ]. For such  $\varepsilon$ , and for  $\ln(Wr/v_0) \gg 1$ , the ratio  $K_0(\varepsilon \tilde{r})/\ln(W/\varepsilon)$  is small in most of the integration domain [ $K_0(x \ll 1) \approx -\log x$ ]. Thus we can Taylor-expand the log and, with logarithmic accuracy, integrate over  $\varepsilon$  using the identity  $\int_0^\infty K_0^2(x) dx = \pi^2/4$ , to obtain

$$U_{AA}(r) = \Omega_{12} \approx \frac{\pi v_0}{4r \log^2(r/\tilde{a})} \cos^2(\mathbf{Kr}). \quad (13)$$

This result is applicable when  $\ln(r/\tilde{a}) \gg 1$ , i.e. when the distance between the adatoms is much larger than lattice constant.

The factor  $\cos^2(\mathbf{Kr})$  in Eq.(13), describing interference between two valleys, takes constant value on each of the three sub-sublattices with period  $\sqrt{3}$  (see Fig.2b). Analyzing it as above we find that  $\cos^2(\mathbf{Kr}) = 1$  for adatoms residing on the same sub-sublattice, and  $\cos^2(\mathbf{Kr}) = 1/4$  when adatoms reside on different sub-sublattices.

The energy of interaction for adatoms on the same sublattice, Eq.(13), is positive, which means that in this case adatoms *repel* each other. This repulsion is logarithmically weaker than the attraction found for atoms on different sublattices, Eq.(11). We thus expect the net interaction for a system of many adatoms randomly placed on both sublattices to be dominated by attraction.

The  $1/r$  interaction of adatoms found in Eqs.(13),(11) is sensitive to the resonant form of the T-matrix. For a small but nonzero detuning  $\delta$  in Eq.(4), we expect the interaction to retain the  $1/r$  form at distances  $r \lesssim \hbar v_0/|\delta|$ , and to decrease faster at larger  $r$ . A similar behavior is expected for a system doped away from neutrality, with spatial cutoff controlled by the Fermi wavelength.

Our next task will be to analyze interaction in a system of adatoms at a finite concentration. Crucially, this interaction is of non-pairwise character, because electronic states with wavelengths exceeding the distance between adatoms,  $\lambda \gtrsim d$ , are strongly perturbed by scattering. In this case, the interaction energy per adatom can be estimated to order of magnitude as  $\varepsilon_* = \hbar v_0/d$ , leading to the  $n^{3/2}$  scaling for the energy density *vs.* adatom concentration, Eq.(1).

This behavior was confirmed by numerical analysis. In the graphene tight-binding problem, we model adatoms by a local potential taking values exceeding  $t_0$ . Given a random configuration of  $N$  adatoms, we diagonalize the Hamiltonian and sum all negative eigenvalues to evaluate the total energy,  $E(N) = \sum_{\varepsilon_\alpha < 0} \varepsilon_\alpha$ . The dependence  $E(N)$  is dominated by a contribution linear in  $N$ , which represents a chemical potential of an adatom. Subtracting the linear part, we recover the interaction  $\Delta E(N) \propto N^{3/2}$  (see Fig.1). Alternatively, one can choose to evaluate  $E(N)$  as a sum over the lower half of

the spectrum. This changes somewhat the linear term, leaving the  $N^{3/2}$  contribution essentially the same.

We performed simulation for a system of size  $48 \times 82$  (Fig. 1). Each data point was averaged over 20 realizations of randomly generated adatom configurations. The data was fitted with the function  $E(N) = E_0 + A_0 N + A_1 N^{3/2}$ . The sign of interaction is that of *attraction* when adatoms are placed with equal probabilities on both sublattices,  $A$  and  $B$ . In this case, the best-fit value of the prefactor in the scaling relation (1) is found to be  $\varepsilon_0 \approx 0.42 t_0$ . With  $t_0 = 3.1$  eV this gives  $\varepsilon_0 \approx 1.3$  eV. In contrast, when all adatoms are placed on one sublattice, a *repulsive* interaction is found; in this case,  $\varepsilon_0 \approx -0.24 t_0 = -0.75$  eV. This is in agreement with the signs of pairwise interaction discussed above.

Next, we test these numerical results against an analytic approach. We use Greens functions found in a self-consistent mean-field approximation, in which point-like adatoms are replaced by a constant field. For disorder-averaged Greens function this approximation yields

$$\tilde{G}^{-1}(i\varepsilon, \mathbf{k}) = i\tilde{\varepsilon} - \begin{pmatrix} 0 & t_{\mathbf{k}} \\ t_{\mathbf{k}}^* & 0 \end{pmatrix}, \quad i\tilde{\varepsilon} = i\varepsilon - \frac{\pi v_0^2 n_1}{i\tilde{\varepsilon} \ln \frac{W}{|\tilde{\varepsilon}|}}, \quad (14)$$

where  $n_1 = 2n/3^{3/2}a^2$  is adatoms' density per sublattice,  $a = 1.42$  Å is carbon spacing. Solving the selfconsistency condition (14) with logarithmic accuracy, we find

$$\tilde{\varepsilon} = \frac{\varepsilon}{2} + \text{sgn } \varepsilon \sqrt{\frac{\varepsilon^2}{4} + \Delta^2}, \quad \Delta^2 \ln \frac{W}{\Delta} = \pi v_0^2 n_1. \quad (15)$$

The energy density of the system can be written as

$$E = \oint \frac{dz}{2\pi i} z \sum_{\alpha} \frac{1}{z - \varepsilon_{\alpha}} = \int_{-\infty}^{\infty} \frac{d\varepsilon}{2\pi} i\varepsilon \text{Tr } G(i\varepsilon) \quad (16)$$

where  $\varepsilon_{\alpha}$  is the spectrum, and the contour integral is taken over the imaginary axis and a half-circle at infinity. The trace of  $G$  is identical to that in the self-energy of a T-matrix, giving  $\text{Tr } G(i\varepsilon) = -2i\tilde{\varepsilon} \ln(W/|\tilde{\varepsilon}|)/\pi v_0^2$ . Subtracting the contribution due to free Dirac fermions, we obtain the change in total energy due to adatoms,

$$E_{\text{int}} = \int_{-\infty}^{\infty} \frac{d\varepsilon}{(\pi v)^2} \varepsilon \left( \tilde{\varepsilon} \ln \frac{W}{|\tilde{\varepsilon}|} - \varepsilon \ln \frac{W}{|\varepsilon|} \right) \quad (17)$$

The function under the integral is even, positive, and approximately constant at  $|\varepsilon| \gtrsim \Delta$ , taking on a value proportional to  $n$  (with logarithmic corrections). At  $0 < \varepsilon \lesssim \Delta$  the function is increasing from zero to the asymptotic value at large  $\varepsilon$ . This behavior is in agreement with expectation of a leading contribution  $\delta E \propto n$  and a *negative*  $n^{3/2}$  part describing interaction. Subtracting the part linear in  $n$ , and dividing by the density of carbon atoms  $n_0$ , we find the interaction energy

$$\Delta E_{\text{int}} = -\frac{8\Delta^3}{3\pi^2 v_0^2 n_0} \left( \ln \frac{W}{\Delta} - \frac{2}{3} \right), \quad n_0 = \frac{4}{3^{3/2} a^2}, \quad (18)$$

per carbon atom. This formula agrees very well with our numerical results (see red curve in Fig.1).

Here it is instructive to make contact with experiment [5]. Long-range attraction between adatoms should lead to thermodynamic instability. This can be seen most easily from phase diagram, obtained from the free energy  $F = E(n) - TS(n)$  (see Fig.1 inset). In our case,

$$F = -\varepsilon_0 n^{3/2} + T(n \ln n + (1-n) \ln(1-n)), \quad (19)$$

giving the critical temperature  $T_* = \varepsilon_0/2\sqrt{3} \approx 4200$  K. Since temperature during hydrogenation is substantially below  $T_*$ , and assuming detailed balance between adsorption and desorption processes, the adatoms tend to self-organize into high and low-density droplets.

Even if spatial diffusion of hydrogen is slow, as may be the case here, regions high and low in hydrogen will form at initial stages of self-organization, before freezing in a low-temperature state. This would lead to macroscopic inhomogeneities of the hydrogenated state. Such inhomogeneities were indeed observed in the TEM diffraction images described in Ref.[5]. It was also noted that dehydrogenation restores homogeneity, pointing to an intrinsic character of this effect.

Also, attraction between “frozen” hydrogen atoms would create a lateral stress

$$\sigma = -\partial E(n)/\partial \ln V \approx \frac{1}{2} |\varepsilon_0| n^{3/2}, \quad (20)$$

where an empirical relation  $\partial t_0/\partial a \approx -t_0/a$  is used to describe the change in  $t_0$ , whereas the occupancy  $n$  is strain-independent. Such stress would lead to compression of the graphene matrix. This is consistent with the reduction in lattice period upon hydrogenation observed by TEM diffraction, which was notably in excess of the value expected from first-principles calculations [5].

In summary, the long-range  $1/r$  interaction makes the behavior of adatoms in graphene rich and interesting. Our predictions agree with the observations of Ref. [5], pointing to the importance of this fundamental interaction in hydrogenated graphene.

We are grateful to A. K. Geim, R. L. Jaffe, and K. S. Novoselov for useful discussions.

---

- [1] A. K. Geim, K. S. Novoselov, *Nat. Mater.* **6**, 183 (2007).
- [2] S. Stankovich *et al.*, *J. Mater. Chem.* **16**, 155 (2006)
- [3] L. Liu *et al.*, *Nano Lett.* **8**, 1965 (2008).
- [4] S. Ryu *et al.*, *Nano Lett.* **8**, 4597 (2008).
- [5] D. C. Elias *et al.*, arXiv:0810.4706
- [6] E. J. Duplock, M. Scheffler, and P. J. D. Lindan, *Phys. Rev. Lett.* **92**, 225502 (2004).
- [7] J. O. Sofo, A. S. Chaudhari, G. D. Barber, *Phys. Rev. B* **75**, 153401 (2007).
- [8] D. W. Boukhvalov, M. I. Katsnelson, A. I. Lichtenstein, *Phys. Rev. B* **77**, 035427 (2008).
- [9] C. Pépin and P. A. Lee, *Phys. Rev. B* **63**, 054502 (2001).
- [10] C. Bena and S. Kivelson, *Phys. Rev. B* **72**, 125432 (2005).

- [11] V. M. Pereira *et al.*, Phys. Rev. Lett. **96**, 036801 (2006).
- [12] M. F. Crommie, C. P. Lutz, and D. M. Eigler, Nature (London) **363**, 524 (1993).
- [13] P. Avouris, Solid State Commun. **92**, 11 (1994).
- [14] J. Repp *et al.*, Phys. Rev. Lett. **85**, 2981 (2000).
- [15] T. L. Einstein and J. R. Schrieffer, Phys. Rev. B **7**, 3629 (1973).
- [16] K. H. Lau and W. Kohn, Surf. Sci. **75**, 69 (1978).
- [17] V. V. Cheianov and V. I. Falko, Phys. Rev. Lett. **97**, 226801 (2006).
- [18] F. Silly *et al.*, Phys. Rev. Lett. **92**, 016101 (2004).
- [19] D. Zhabinskaya, J. M. Kinder, E. J. Mele, arXiv:0812.1990
- [20] M. Bonfanti, R. Martinazzo, G. F. Tantardini, and A. Ponti, J. Phys. Chem. C **111**, 5825 (2007)
- [21] J. C. Meyer, C. O. Girit, M. F. Crommie, A. Zettl, Nature **454**, 319 (2008).
- [22] A. A. Abrikosov, L. P. Gor'kov and I. E. Dzyaloshinsky, Methods of Quantum Field Theory in Statistical Physics (Dover, New York, 1975).
- [23] T. Emig, N. Graham, R. L. Jaffe, and M. Kardar, Phys. Rev. Lett. **99**, 170403 (2007).
- [24] O. Kenneth, I. Klich, Phys. Rev. B **78**, 014103 (2008).